

# Finite element study on bond behavior of steel bar and HSCC/HSFRCC

A.K.F. Cheung & C.K.Y. Leung

*Hong Kong University of Science and Technology, Hong Kong, China SAR*

P. Kabele

*Czech Technical University in Prague, Prague, Czech Republic*

**ABSTRACT:** To study the bond behavior of steel bar and High Strength Cementitious Composites (HSCC) or High Strength Fiber Reinforced Cementitious Composites (HSFRCC), finite element simulations of Direct Tension Pull-out Bond Test (DTP-BT) are conducted. Default tensile strain softening relation in FE program ATENA is used to model HSCC. Satisfactory agreement between simulated and experimental load-displacement curve can be obtained by taking specific fracture energy of HSCC to be 50 N/m. Similar to experimental observations, tensile splitting failure is shown to be the dominate failure mode. To simulate the behavior of HSFRCC members, either the homogenization based approach (H-model) or individual crack based approach (I-model) can be employed to describe the tensile strain hardening behavior. In this paper, both approaches are first presented and discussed. Numerical results are compared to experimental results obtained in our laboratory. According to our findings, the pre-peak behavior of DTP-BT can be properly simulated by the I-model. On the other hand, H-model shows overestimation of pre-peak stiffness. Similar to HSCC, tensile splitting failure is the dominate failure mode of HSFRCC DTP-BT member. From the tests, the width of the splitting crack is wider at the surface than at the steel level. This can be explained by the numerical simulation which shows very high tensile stress at the surface of the DTP-BT specimen.

## 1 INTRODUCTION

High strength fiber reinforced cementitious composites (HSFRCC) are cementitious materials with high stiffness (Elastic modulus: 38-45GPa) and compressive strength (150-200MPa). Due to the high brittleness of the cementitious matrix in this kind of material, micro steel fiber is added to enhance ductility and to prevent sudden failure. With sufficient amount of fiber (2% in volume fraction), HSFRCC exhibits strain hardening behavior under uniform tensile stress. Unlike ECC, a very ductile cementitious composite, which can sustain increasing tensile load for tensile strain beyond 5%, HSFRCC may exhibit hardening behavior up to a strain of 0.5%. With crack bridging fibers transmitting stress back into the matrix, some multiple cracking can be observed.

With high mechanical strength and toughness, HSFRCC can be used as a joining material to shorten the width of joint between precast concrete beam/slabs. Bond behavior of steel bar embedded in HSFRCC has been experimentally investigated by Cheung & Leung (2008) with the Direct Tension Pull-out Bond Test (DTP-BT), and tensile splitting failure was found to be the dominant failure mode for embedment lengths of 5d and 8d. Due to tensile load transfer of the pulled bar, compressive stresses

is generated in the cementitious composite bordering the load bearing area of the bar. As a result, tensile hoop stresses are generated to induce splitting failure. Prediction of the splitting failure load is complicated as it is affected by many parameters, including concrete compressive strength, diameter and embedment length of the steel bar, as well as the distance of bar to the member surface (Hüer & Eligehausen 2007).

Numerical simulation can be a useful aid to analyze the bond failure process and to predict the ultimate failure load. For nonlinear analysis of bond failure, the finite element method (FEM) is most commonly used in conjunction with proper constitutive models representing the mechanical behavior of corresponding materials. In this study, finite element analysis of bond behavior between steel bar and HSCC/HSFRCC is investigated (Note: HSCC stands for high strength cementitious composites without fiber). DTP-BT with embedment length 5d is modeled. Default concrete model in ATENA is used for HSCC. Using fracture energy of 75N/m and 50N/m, the simulated load-displacement behavior and failure mode are compared to experimental result. HSFRCC is a strain hardening cementitious composites, so a constitutive model that can describe the tensile pseudo-strain hardening

as well as subsequent localized fracture and softening is required. During strain hardening, multiple cracks will form along the member. In the homogenization based approach, the multiple cracks are not explicitly considered and the stress vs strain behavior is simply fitted with a multilinear relation as shown in Figure 1. However according to Kabele (2009), the homogenization based approach may sometimes overestimate the prepeak stiffness especially when the strain hardening cementitious composites is exposed to a complex non-proportional loading history. An individual crack based approach was therefore proposed to enable a more accurate simulation of experimental results. In this study, experimental results from HSFRC members are simulated by both homogenization based model and individual crack based model.

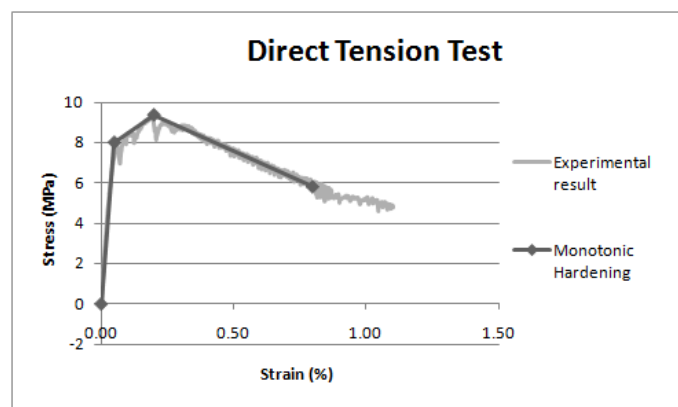


Figure 1. Tensile stress strain curve of HSFRC and monotonic hardening model.

## 2 FINITE ELEMENT CODE

The finite element (FE) program ATENA (Červenka, 2008) employed in this study uses the fracture-plastic model to represent cementitious materials with low tensile strength and high compressive strength. The fracture-plastic model is a combination of constitutive models for tensile (fracturing) and compressive (plastic) behavior (Červenka & Papanikolaou 2008). In tension, the fracture model is based on the classical orthotropic smeared crack formulation and crack band model. It employs Rankine failure criterion, exponential softening, and can incorporate both rotated and fixed cracks. In compression, the hardening/softening plasticity model is based on Menétrey-Willam or Drucker-Prager failure surface. Similar to other FE programs, default concrete model is available in ATENA. However, for some newly developed cementitious composites such as ECC (Li 2003) or HSFRC, the stress-strain relationship differs from conventional concrete as significant strain hardening occurs under tensile loading. To simulate the strain hardening behavior of HSFRC in tension together with its strain

softening behavior in compression, the user defined model of the program is employed.

## 3 FINITE ELEMENT MODEL

### 3.1 Analysis of HSCC-steel bond behavior

#### 3.1.1 Material properties

The 3D Nonlinear Cementitious 2 Model of ATENA is used to simulate the material properties of HSCC. Young's modulus  $E_c$  of 38000MPa and Poisson's ratio  $\nu_c$  of 0.2 are taken to be the material properties of high strength concrete. The tensile strength of HSCC in the model is 8MPa based on the experimental results from Direct Tension Test. The cube compressive strength of HSCC is 150MPa. In the program, the defined cube compressive strength is automatically converted to cylindrical compressive strength by a multiplying factor of 0.85.

In this work, the fracture energy of HSCC has not been measured directly and an estimate of its value is required. Marzouk (1995) reported that high strength concrete has a more brittle and stiffer behavior than normal strength concrete. After peak load, the stress-deformation curve descends more sharply than that of normal strength concrete. According to Zhou et al. (1995), the fracture energy of high strength concrete increases with increasing aggregate size and with increasing aggregate stiffness. Zhang (2005) found the fracture energy and characteristic length to increase with increasing coarse aggregate size in both normal and high strength concretes. However, the effect of coarse aggregate size on the shape of stress-deformation curve is not significant in high strength concrete, as most cracks tend to cut through the aggregate due to the improved aggregate-matrix bonding at the interface. The fracture energy hence depends on the properties of aggregates used, and is normally within the range of 100-200 N/m. However, for high strength cementitious materials with only fine sand but no aggregates, the fracture energy can be lower. For a plain reactive powder concrete (RPC) with quartz sand within 0.15-0.63mm and sand/cement ratio of 1.51, Ju et al. (2009) obtained compressive strength of 157MPa and fracture energy 75N/m. For the HSCC in our experimental study, maximum size of silica sand used is 1.2mm and the sand/cement ratio is about 0.86. While the sand size is a bit higher than the RPC, the sand/cement ratio is lower. We therefore assume the fracture energy of the HSCC to be similar to or lower than the RPC. In the FE model of DTP-BT, the specific fracture energy of HSCC was taken to be 50N/m and 75 N/m to see how the numerical results compared to the test data.

### 3.1.2 Model of DTP-BT

DTP-BT was conducted to study the pull-out behavior of steel bar embedded in HSCC. A steel bar with diameter of 16mm was embedded in a prismatic specimen with dimensions 360mm x 120mm x 120mm. To simulate the pull-out behavior of steel bar in HSCC, triple symmetry was assumed and one-eighth of the specimen was modeled. All constituents of the model were discretized by four-node brick elements with the meshing shown in Figure 2. The embedment depth of the pull-out bar was 80mm length (5d). The behavior of the bar was assumed to be elastic perfectly plastic with a Young's modulus  $E_s$  of 210GPa and yield strength  $\sigma_s$  of 500MPa. In this model, perfect bonding between the steel bar and HSCC was assumed, because failure in the tested specimens were due to concrete splitting rather than interfacial sliding. If perfect bonding is assumed, the Poisson's effect of steel bar could affect the result. In this work, the Poisson's ratio was taken to be zero. The bar was discretized by four-node tetrahedral elements. To prevent tensile cracking of the test specimen, four 12mm diameter high yield steel bars were placed near the corners. The corner bar was considered in the model. It was assumed to exhibit linear elastic behavior with  $E_s$  of 210GPa and Poisson's ratio  $\nu_s$  of 0.2. To simulate displacement-controlled loading of the specimen during the test, fixed incremental displacement was applied on the upper surface of the pull-out bar in each load step.

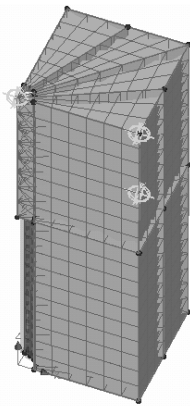


Figure 2. FEM models of DTP-BT.

## 3.2 FEM of HSFRC-steel bond behavior

### 3.2.1 Material properties

The 3D Nonlinear Cementitious 2 User Model of ATENA is used to describe the material properties of HSFRC. The Young's modulus  $E_c$ , Poisson's ratio  $\nu_c$ , tensile strength  $\sigma_t$  and compressive strength  $\sigma_c$  are taken to be the same as the HSCC. The configuration of the DTP-BT model, element types and element size are the same as those described in the previous section. The main difference of HSFRC model and HSCC model is the description of tensile stress strain relationship. The tensile stress

strain relationship of HSCC model depends on the specific fracture energy which governs its strain softening behavior. With this model, strain hardening behavior cannot be described. To consider strain hardening for the HSFRC, a user defined stress strain relationship is employed. Kabele (2009) illustrated the simulation of strain hardening cementitious composites by both homogenization based model and individual crack based model. Individual crack based model was found to have more accurate simulation of the pre-peak behavior of an ECC shear beam. In this study, simulation of the HSFRC DTP-BT is also performed with both the homogenization based model and individual crack based model. The results will then be compared.

### 3.2.2 Homogenization based model (H-Model)

Figure 1 shows the stress strain relationship of HSFRC with 2% micro steel fiber in volume, measured from the direct tension test. After first cracking, strain hardening up to a tensile strain of about 0.2% can be observed. The strain hardening behavior is resulted from bridging of the crack by micro steel fibers which transfer stresses back to the adjacent matrix, causing formation of new cracks. The multi-linear tensile stress strain relationship obtained from fitting of experimental test can be directly applied in the FEM model. Figure 3 shows the defined stress strain relationship of H-Model and I-Model in tension after first cracking. The figure does not show the linear elastic part because only the stress strain behavior after first crack is required to be defined in the program. The elastic behavior is calculated based on other material parameters (i.e. Young's modulus  $E_c$  and tensile strength  $\sigma_t$ ). The strain hardening part of H-Model is obtained from the fitting of experimental result of the direct tension test. The ratio of peak strength and tensile strength is 1.17 as shown in the experimental curve. As the post peak behavior describes the gradual loss of bridging capacity due to fiber pull-out, the theoretical curve should be of a concave shape. However, as shown by the test data in Figure 1, the softening behavior up to 1% strain appears to be rather linear. To simplify the simulation, the post-peak behavior of HSFRC is therefore approximated by a linear softening relationship (Kabele 2009). The post-peak  $\sigma$ - $\delta$  law can be calculated by:

$$\sigma(\delta) = \sigma_0 \left( 1 - \frac{\delta - \delta_0}{\delta_F - \delta_0} \right) \quad \text{for } \delta_0 \leq \delta \leq \delta_F$$

where  $\sigma_0$  is peak strength,  $\delta_0$  is the crack opening displacement (COD) at  $\sigma_0$  and  $\delta_F$  is COD at zero stress which is estimated from the linear softening slope of tensile stress strain curve. It is assumed that a set of cracks, perpendicular to the principal stress

direction, will form once the maximum principal stress goes beyond the first cracking strength. The overall material response normal to the crack is governed by a linear hardening relationship until the ultimate tensile strength is reached.

### 3.2.3 Individual crack based model (I-Model)

The response of an opening crack in the HSFRC is governed by the cohesive effect of matrix and the bridging effect of fibers. Due to the high brittleness of the matrix of HSFRC, a linear tension-softening relationship is usually assumed to describe crack opening response of the matrix. The linear tension softening relationship is determined by two parameters which are the cracking strength  $\sigma_{Mc}$  and the COD  $\delta_{M0}$  at which the matrix cohesion is completely lost:

$$\sigma_M(\delta) = \sigma_{Mc} \left( 1 - \frac{\delta}{\delta_{M0}} \right) \quad \text{for } \delta \leq \delta_{M0} \quad (1)$$

Note that the matrix fracture energy is

$$G_M = \frac{1}{2} \sigma_{Mc} \delta_{M0}$$

Before the bridging of fiber become effective,  $\sigma_M$  keeps decreasing according to equation (1). With higher brittleness, the decrease of stress for high strength matrix is more rapid than that for normal strength concrete. Based on the deduced  $\sigma$ - $\delta$  relationship in Zhang et al. (2005),  $d\sigma/d\delta$  for the matrix in HSFRC is estimated to be  $-187 \text{ N/mm}^3$ .

Strain hardening behavior of HSFRC in tension is resulted from fiber bridging at the cracks. To consider each crack individually, a bridging stress vs crack opening relationship can be derived from micromechanics. According to Li (1992), the bridging stress for opening cracks can be related to the COD  $\delta$  by following equation:

$$\sigma_b(\delta) = \sigma_0 \left[ 2 \left( \frac{\delta}{\delta_0} \right)^{\frac{1}{2}} - \frac{\delta}{\delta_0} \right] \quad \text{for } \delta \leq \delta_0 \quad (2)$$

where  $\sigma_0$  is the maximum stress that can be carried by fiber bridging and  $\delta_0$  is the COD at the maximum bridging stress. In this study,  $\delta_0$  of fiber reinforced cementitious composites is estimated to be about  $100 \mu\text{m}$ . With equation (2) describing the behavior at each crack, the bridging stress strain relationship in tension can be calculated. The post-peak  $\sigma$ - $\delta$  law can be calculated as described in the previous section. Based on the above discussions, the complete  $\sigma$ - $\delta$  relationship for the individual crack based model can be obtained by combining the

curves from equations (1) and (2) and assuming linear softening after the ultimate load  $\sigma_0$  is reached.

$$\sigma(\delta) = \sigma_{Mc} \left( 1 - \frac{\delta}{\delta_{M0}} \right) \quad \text{for } \delta \leq \delta_b$$

$$\sigma(\delta) = \sigma_0 \left[ 2 \left( \frac{\delta}{\delta_0} \right)^{\frac{1}{2}} - \frac{\delta}{\delta_0} \right] \quad \text{for } \delta_b \leq \delta \leq \delta_0$$

$$\sigma(\delta) = \sigma_0 \left( 1 - \frac{\delta - \delta_0}{\delta_F - \delta_0} \right) \quad \text{for } \delta_0 \leq \delta \leq \delta_F$$

In the above,  $\delta_b$  is the COD at which equation (1) and (2) intersects. In ATENA,  $\sigma/\sigma_{MC}$ - $\varepsilon$  relationship is used to describe the behavior of elements after first cracking. Therefore, the  $\sigma$ - $\delta$  relationship has to be converted to a  $\sigma/\sigma_{MC}$ - $\varepsilon$  relationship for H-Model and I-Model by the known element size and characteristic size, both being 10mm in this analysis. The tensile stress strain relationships for both H-Model and I-Model are shown in Figure 3. It can be observed that the I-Model shows a rapid drop in stress due to matrix cracking, followed by a gradual increase while the fibers are picking up the stress.

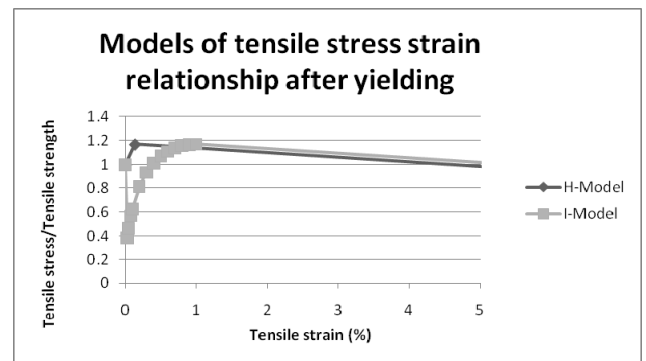


Figure 3. Tensile stress strain relationships of H-Model and I-Model.

## 4 NUMERICAL ANALYSIS

The main purpose of the 3D FE analysis was to investigate the ultimate capacity, structural behavior and failure mode for DTP-BT of HSCC and HSFRC specimens with steel embedment depth of 5d. In the numerical study, we will focus on the load-displacement curves and crack patterns. For HSCC DTP-BT model, the influence of specific fracture energy is studied by comparing the ultimate capacity of the models. To investigate the FE simulation of HSFRC in DTP-BT, both H-model and I-model are employed. The accuracy of the simulations is shown by the comparison of load-displacement curves with test results.

#### 4.1 HSCC DTP-BT model

The load-displacement curves of HSCC DTP-BT models with specific fracture energy of 75N/m (HSCC DTP-BT-75N/m) and 50N/m (HSCC DTP-BT-50N/m) are shown together with the experimental result in Figure 4. The experimental curve showed a nearly linear pre-peak behavior up to the peak load of 40.5kN and a sudden drop of load after the peak load. The numerically obtained peak loads from HSCC DTP-BT-75N/m model and HSCC DTP-BT-50N/m model are respectively 35% and 13% higher than the experimental result. The results indicate that the fracture energy of HSCC is a critical parameter to determine the ultimate capacity of the test. Although the fracture energy of HSCC has not been found experimentally, it is reasonable to estimate the value to be lower than that of RPC (which is 75N/m) as discussed in the previous section. In the analysis, even when fracture energy of 50N/m was used, the peak load was still overestimated. The overestimation can be due to many reasons. One of them is the neglecting of the wedging action from the ribs to the splitting of HSCC matrix in the FEM models because the wedging action can weaken the splitting resistance of HSCC. However, generally speaking, the simulated structural behavior of HSCC DTP-BT still shows reasonable agreement with experimental curve. Similar to the experimental curve, the modeling results show a sudden drop of load after the peak load. Although the post-peak load drop is occurring slower, the overall trend is similar. The gradual load decrease in the model could be due to the assumption of perfect bond between steel bar and HSCC matrix. Load can still be transferred from the steel bar to the matrix at the regions of splitting tensile crack even after crack propagation has reduced the friction between the concrete and steel. While further refinement can certainly be made for the FE models, the HSCC DTP-BT-50N/m model appears to provide a satisfactory simulation of the load-displacement behavior.

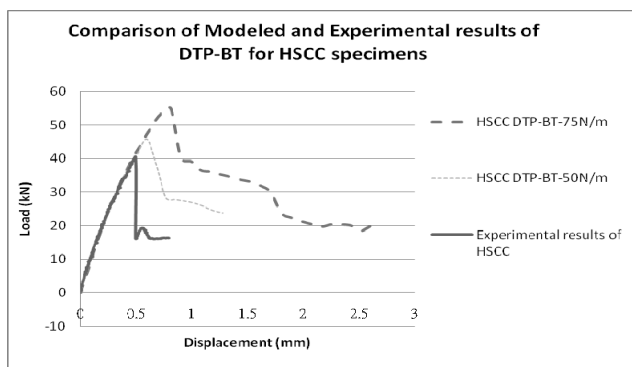


Figure 4. Load-displacement curves of HSCC models and experimental results.

According to the experimental observations on DTP-BT specimens, the failure is governed by the splitting of HSCC. However, as there is neither fiber nor confining steel bar in the HSCC DTP-BT specimen, the failure occurs suddenly and the HSCC at the loaded zone broke into several pieces. Therefore, the propagation of splitting crack is difficult to observe in the experiment. By the FE analysis of DTP-BT, the development of crack can be studied. Crack width plot and the crack pattern of HSCC DTP-BT-75N/m and HSCC DTP-BT-50N/m models at peak load are shown respectively in Figure 5 and Figure 6. To have better understanding of the crack propagation, crack width plot and crack pattern of different cross sections from top surface to 40mm from the top are shown in the figures. There are two kinds of cracking that can be identified in the figures. One is the localized cracks along the interface between steel pull-out bar and HSCC specimen and another is the tensile splitting crack. The localized cracks developed along the interface between steel bar and HSCC specimen. From the crack width plot, the width of localized cracks around the steel bar is much larger. However, due to the rapid decrease of tensile stress away from the steel bar towards the outer surfaces of the specimen, these localized cracks stop propagating and will not govern the failure. From the crack patterns shown in Figure 5 and Figure 6, the tensile splitting crack initiates from the steel pull-out bar on the top surface and propagates towards the surface on the side. After the peak load, the crack on the top continues to propagate while additional tensile splitting cracks also initiate from the steel bar below the top surface and propagate outwards. The simulation is therefore able to identify the splitting failure process in the DTP-BT test.

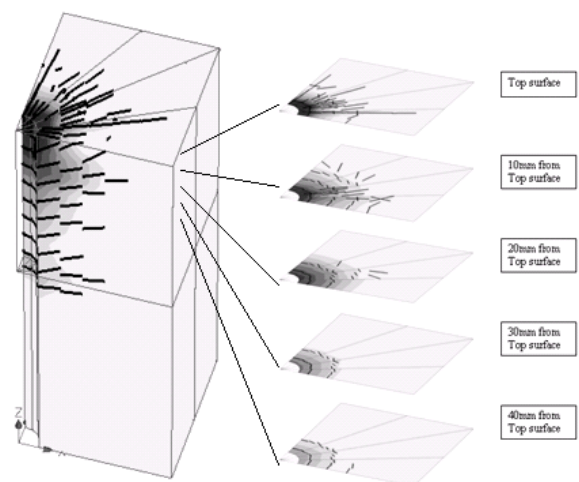


Figure 5. Crack width plot and crack pattern at peak load of HSCC DTP-BT-75N/m model.

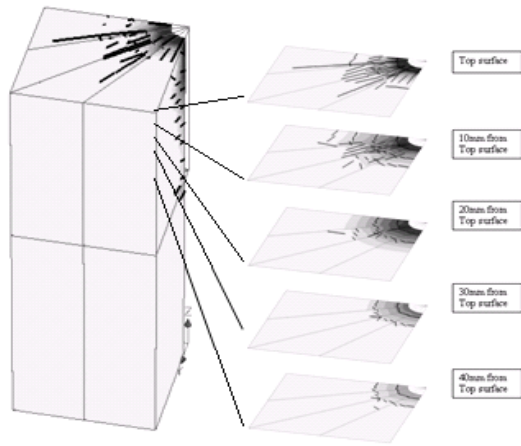


Figure 6. Crack width plot and crack pattern at peak load of HSCC DTP-BT-50N/m model.

#### 4.2 HSFRC DTP-BT model

The load-displacement curves of H-model and I-model as well as the experimental result for HSFRC specimen are shown in Figure 7. Nonlinear behavior before yielding of steel pull-out bar was observed from experimental load-displacement curve. The load stayed constant after yielding of steel bar and finally a drop of load was recorded due to splitting failure of the HSFRC specimen. The FE analysis using H-model to simulate the strain hardening of HSFRC shows an almost linear elastic behavior before the yielding of steel pull-out bar. Similar to the conclusion from Kabele (2009), overestimation of pre-peak stiffness and load (for a given displacements) is resulted if H-model is used to represent the strain hardening behavior. The load-displacement of I-model shows a good agreement to the experimental result. Non-linear behavior before yielding of steel pull-out bar can be captured. Unlike H-model, I-model shows a good estimation of pre-peak behavior of DTP-BT by deriving the tensile stress strain relation according to the fiber bridging relation at a crack when the strain hardening behavior of HSFRC is developed.

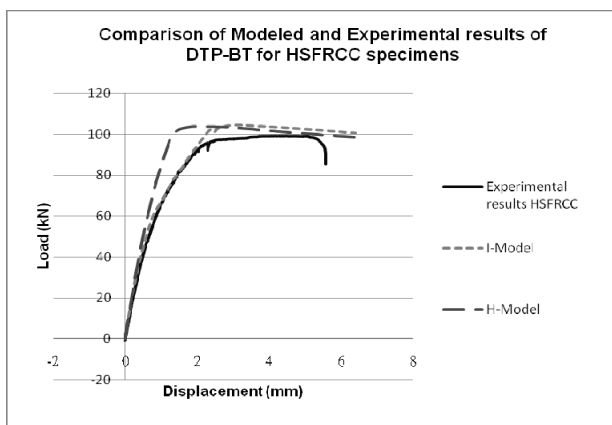


Figure 7. Load-displacement curves of H-model, I-model and experimental results.

During the bond test, the failure mode of HSFRC specimen was found to be tensile splitting failure (Fig. 8). From the figure, a major crack is identified on the top surface of DTP-BT specimen. The crack width of the major crack at the specimen surface is similar or even larger than the crack width adjacent to the steel bar. However the splitting crack is initiated from the steel pull-out bar and propagates to the side surface. If the crack open up further during the pull out of steel bar, the crack width adjacent to the steel bar should be larger. To understand the process of tensile splitting, crack width plots and crack patterns of H-model and I-model at the peak load are shown in Figure 9 and Figure 10. Similar to the DTP-BT model of HSCC, two kinds of cracks can be identified, i.e. localized crack and tensile splitting crack. From the crack width plot in the figures, the crack width at the zone of localized crack (along steel pull-out bar) is larger than those of splitting tensile crack. However, the failure of DTP-BT specimen is not governed by the localized crack. The tensile splitting crack on the top surface can be identified in the figures. Similar to the case of HSCC, this crack is initiated from the steel bar and propagates to the side on the top surface. However, for the cross section 10mm below top surface in Figure 9 and the cross sections 10mm and 20mm below top surface in Figure 10, initiation of splitting crack from the outside can also be observed. According to the numerical result, the surface crack is initiated by high tensile stress along the side of the specimen as shown in Figure 11. The opening of the surface crack and its propagation towards the steel bar can explain the wider crack width observed on the surface of the DTP-BT specimen.



Figure 8. Tensile splitting failure of HSFRC under DTP-BT.

## 5 CONCLUSION

Finite element analysis of bond behavior between steel bar and HSCC or HSFRC is studied with the FE program ATENA. For HSCC samples under Direct Tension Pull-out Bond Test (DTP-BT), tensile splitting failure is shown to be the dominant failure mode. The tensile splitting crack is initiated from the steel pull-out bar and propagates to the surface on the side. The peak load of DTP-BT is sensitive to the specific fracture energy of the HSCC. The numerical analysis shows that fracture energy of 50N/m can give a satisfactory simulation of the experimental results.

To simulate DTP-BT test on HSFRC specimens, the description of strain hardening behavior by two different approaches: a) Homogenization based approach (H-model) and b) Individual crack based approach (I-model) is investigated and compared. From the numerical results, H-model shows linear pre-peak behavior before steel yielding and over-estimation of pre-peak stiffness for load-displacement curve. I-model shows nonlinear pre-peak behavior in very good agreement to the experimental result. Both models show similar failure mode, i.e. tensile splitting failure. Similar to HSCC, the splitting tensile crack on the top surface is initiated from the steel bar and propagates to the surfaces at the sides. However, crack opening is more controlled and ductility is enhanced by the fiber bridging. From numerical analysis, the tensile stress generated at the side surface during pull-out of steel bar can induce the formation of surface crack and its opening and propagation towards the steel bar. This explains the wider crack width at the surface of HSFRC DTP-BT specimen observed in the experiment.

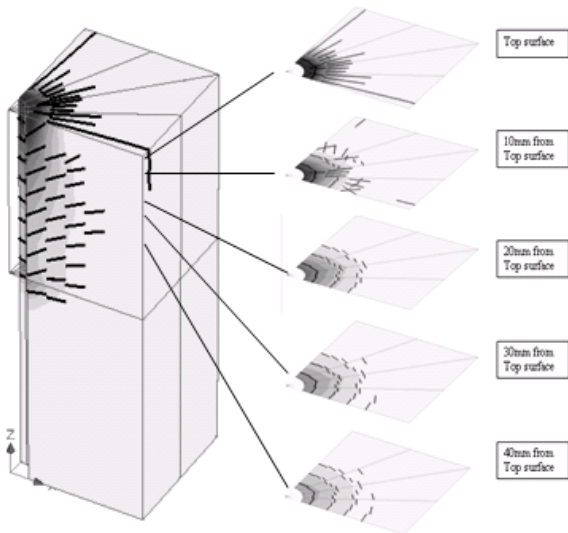


Figure 9. Crack width plot and crack pattern at peak load of H-model.

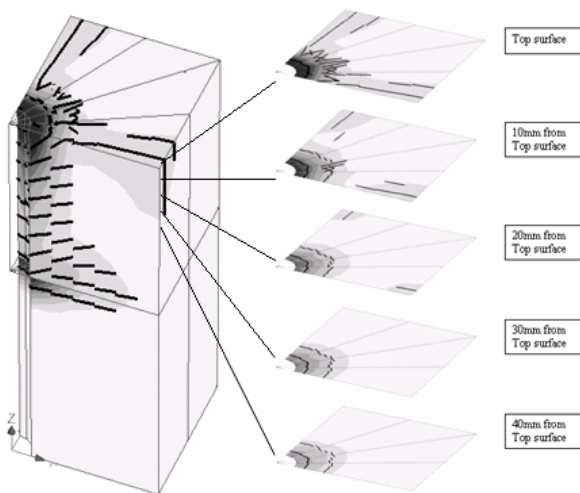


Figure 10. Crack width plot and crack pattern at peak load of I-model.

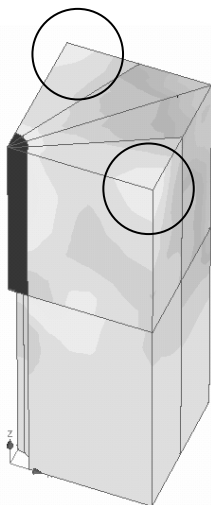


Figure 11. Principal stress plot of I-model.

## REFERENCES

- Červenka, J. & Papanikolaou, V.K. 2008. Three dimensional combined fracture-plastic material model for concrete. *International Journal of Plasticity* 24 (12): 2192-2220.
- Červenka, V., Jendele, L. & Červenka, J. 2008. *Atena program documentation, part 1, theory*. Prague: Červenka Consulting.
- Cheung, A.K.F., Leung, C.K.Y. 2008. Experimental study on the bond between steel reinforcement and self-compacting high strength fiber reinforced cementitious composites, *Seventh International RILEM Symposium on Fibre Reinforced Concrete: Design and Applications BEFIB*, 667-678.
- Hüer, T., Eligehausen, R. 2007. Splitting failure mode of bonded anchors, *Fracture Mechanics of Concrete Structures – Design, Assessment and Retrofitting of RC Structures*, 753-760.
- Ju, Y., Liu, H.B., Chen, J., Jia, Y.D., Peng P.H. 2009. Toughness and characterization of reactive powder concrete with ultra high strength. *Sci China Ser E-Tech Sci*, 52 (4), 1000-1018.

- Kabele, P. 2009. Finite element fracture analysis of reinforced SHCC members, International Conference Advanced Concrete Materials, Stellenbosch, South Africa.
- Li, V.C. 1992. Post-crack scaling relations for fiber-reinforced cementitious composites, ASCE Journal of Materials in Civil Engineering, 4 (1), 41-57.
- Li, V.C. 2003. On engineered cementitious composites (ECC) – a review of the material and its applications. Journal of Advanced Concrete Technology 1 (3): 215-230.
- Marzouk, H., Chen, Z.W. 1995. Fracture energy and tension properties of high-strength concrete. Journal of Materials in Civil Engineering, (5), 108-115.
- Zhang, J., Liu, Q., Wang, L. 2005. Effect of coarse aggregate size on relationship between stress and crack opening in normal and high strength concretes, Journal of Material Science and Technology, 21 (5), 691-700.
- Zhou, F.P., Barr, B.I.G., Lydon, F.D. 1995. Fracture properties of high strength concrete with varying silica fume content and aggregates. Cement and Concrete Research, 25 (3), 543-552.